Korean J. Chem. Eng., 35(1), 12-19 (2018)
DOI: 10.1007/s11814-017-0263-2
pISSN: 0256-1115
eISSN: 1975-7220

RAPID COMMUNICATION

Synthesis, characterization and electrical properties of polypyrrole/V_2O_5 composites

Khan Malook*,, Hamayun Khan*,†, Mutabar Shah***, and Ihsan-Ul-Haque****

*Department of Chemistry, Islamia College University, Peshawar 25120, Pakistan
**Centralized Resource Laboratory, University of Peshawar, Peshawar 25120, Pakistan
***Department of Physics, University of Peshawar, Peshawar 25120, Pakistan
(*Received 30 January 2017 • accepted 21 September 2017*)

Abstract−Polypyrrole (PPy) and its composites with vanadium pentoxide (V_2O_5) were synthesized in aqueous medium by chemical oxidation polymerization using $FeCl_3 \cdot 6H_2O$ as an oxidant. The materials were characterized by Fourier transform infrared (FT-IR) spectroscopy, X-ray diffractometry (XRD), thermogravimetry analyzer (TGA), scanning electron microscopy (SEM), energy dispersive X-ray (EDX), UV/visible spectroscopic techniques and LCR-meter. The FT-IR results confirmed the successful synthesis of PPy and PPy/V_2O_5 composites. The XRD study showed the amorphous and crystalline nature of PPy and PPy/V_2O_5 composites, respectively. The TGA analysis showed slight increase in the thermal stability of the composites. The SEM data verified the porous nature of PPy and the composites. The UV/visible spectrometry confirmed the doping of PPy in composites. The electrical properties of the materials displayed their semiconducting nature. The resistance of the samples was found to be dependent on temperature and the contents of V_2O_5 in the composites.

Keywords: Polypyrrole, V_2O_5, Composite, Polymerization, Analytical Characterization, Electrical Properties

INTRODUCTION

Intrinsically conducting polymers (ICPs) have been widely used as synthetic metals because they can be the best alternative for semiconductors and metals in different electronic and electrical devices while retaining conventional polymeric properties [1]. The characteristics of these polymers such as high thermal and air stability, ease of preparation and process scale-up, electrochemical characteristics, biocompatibility, electrical properties, and reversibility are the basis for their analytical, technological and commercial uses [2]. Due to their greater electrical conductivity, ICPs have been widely used as basic materials for advanced applications such as batteries, EMI shields, light emitting diodes, gas separation membranes, electrochromic devices, smart windows, and biochemical sensors [3-10].

However, ICPs are chemically stable, brittle and infusible materials which suffer from poor processibilty due to their very stiff conjugated back bone structures [11-14]. The applications of these polymers in some other fields are limited because of their poor mechanical strength [15]. Similarly, in other fields, the higher conductivity of these polymers is not sufficient. For example, using these polymers as a gas sensor faces the problem of long response/recovery time, lower sensitivity and poor dynamic response as compared to their composites with metal oxides [16,17]. For these reasons, there is need to synthesize polymer based organic-inorganic composites in which organic components are ICPs and various metal oxides as inorganic counterpart. These composite materials have greater thermal and chemical stability and ability to retain charge along with attractive physical and mechanical properties [18-20]. Boyano et al. [21] prepared PPy/V_2O_5 hybrid composites with and without pyridine sulfonic acid (PSA) as additive and found 20% increase in the charge storage ability of the material using PSA when applied as a cathode in lithium ion battery. Kuwabata et al. [22] synthesized PPy/V_2O_5 composites by chemical polymerization of Py monomer in the presence of V_2O_5. The materials showed better charge-discharge capacity as compared to the individual components. Sun et al. [23] produced V_2O_5 nanofibers (Nfs) wrapped with PPy by a two-step method. The work claimed the groundwork for understanding the synergistic effect and individual performance of each component of hybrid electrode materials. Rahman et al. [24] compared the AC conductivity of PPy and PPy/V_2O_5 nanocomposites. The PPy showed greater AC conductivity than the composites due to smaller d-spacing.

PPy in oxidized form is one of the ICPs which have recently received greater attention of researchers' due to their simple preparation methods and higher conductivity approaching to that of metals in certain cases [25]. A reasonable amount of PPy having charge carriers on its back bone can be obtained as black powder using chemical or electrochemical polymerization methods from Py in the aqueous or other medium. The charge carriers move across and along the polymer chain that is responsible for its conducting behavior. The polymeric chain of PPy has conjugated bond stabilized by incorporated counter anions [26]. The counter ions are generally the anions of the oxidant. For example, when PPy is synthesized by chemical oxidation polymerization method using $FeCl_3$ as an oxidant and the chloride ions are incorporated as counter ions into the polymer matrix [27].

However, like other ICPs, PPy also faces the same limitations as

†To whom correspondence should be addressed.
E-mail: hamayun84@yahoo.com

mentioned above. To get rid of those limitations and to improve its properties, there is need to prepare its composite with various inorganic materials such as metal oxides. V_2O_5 is a semiconducting transition metal oxide with band gap around 2.0 eV [28]. Its unique layered structure makes it an important material for various applications such as catalyst, lithium ions batteries, electronic devices and supercapacitors [29]. Keeping in view the important characteristics of PPy, V_2O_5 and polymer-metal oxide based composites, the present work was under taken. In this study, PPy and its composites with V_2O_5 were prepared by a chemical oxidation polymerization method reported for the preparation of PPy/ZnO_2 composites [30]. However, we used smaller concentrations of the reactants to get composites having a thin deposited layer of PPy over V_2O_5 particles where both of the components of the composites will have significant contribution in directing their properties. All the samples were characterized and their electrical properties were determined for possible applications in electronic devices.

Fig. 1. Schematic presentation of the experimental setup for the synthesis of PPy and PPy/V_2O_5 composites.

MATERIALS AND METHODS

1. Materials

Analytical grade chemicals were used. The Py, the oxidant ($FeCl_3 \cdot 6H_2O$), acetone, ethanol and V_2O_5 were purchased from Merck (Germany). The Py after distillation under reduced pressure was kept in dark till further use. The solutions were prepared in deionized double distilled water (DDDW) (UVF, ELGA Milli-Q Water System, UK).

2. Synthesis of PPy

PPy was obtained by chemical oxidation polymerization of Py. Briefly, 1 M aqueous solution of Py was added slowly into the aqueous $FeCl_3 \cdot 6H_2O$ solution (0.1 M) with continuous magnetic bar stirring and nitrogen flow for 2 h at 8 °C. A black color precipitate obtained as a result of the polymerization of Py was filtered under vacuum followed by washing with sufficient volume of DDDW, ethanol, acetone. The product so obtained was desiccated at 40 °C for 4 h and then stored in a desiccator.

3. Synthesis of PPy/V_2O_5 Composites

The V_2O_5 (0.2 g) was dispersed in 0.1 M aqueous $FeCl_3 \cdot 6H_2O$ solution and sonicated for 30 min. Then 1 M solution of Py was added slowly to the above mixture under swirling condition. The mixture was stirred for 2 h to obtain PPy/V_2O_5 composite and was termed as PPy/2%V_2O_5. The other composites (PPy/5%V_2O_5, PPy/8%V_2O_5 and PPy/10%V_2O_5) were also prepared under the same conditions; however, the amount of V_2O_5 was increased, i.e., 0.5, 0.8 and 1 g, respectively. A schematic diagram of the experimental setup for the preparation of PPy and PPy/V_2O_5 composites is shown in Fig. 1.

4. Characterizations

The samples were characterized using various techniques including Fourier transform infra-red (FT-IR) spectroscopy, X-ray diffraction (XRD) spectroscopy, thermogravimetric analysis (TGA), scanning electron microscopy (SEM), energy dispersive X-ray (EDX) spectroscopy and LCR-meter. For FT-IR data, an appropriate quantity of the samples was mixed with KBr (IR grade), and small quantities of the samples were transferred to a sample cup of the diffuse reflectance accessory (DRS-8000 A) for scanning purpose. FT-IR spectral analyses were performed by FT-IR spectrometer (FT-IR-8400, Shimadzu, Japan) with wavenumber varying from 400 to 4,000 cm^{-1}. The powder XRD analyses of the samples involved a JEOL JDX-9C-XRD (Japan) spectrometer with Cu K_α radiations. The scanning range of each sample was 2θ of 10 to 80° with scan speed of 0.1°/sec and step angle of 0.05°, while the tube voltage and current were 40 kV and 30 mA, respectively. The TGA study of the samples was performed by a PerkinElmer Diamond TG/DTA (USA). For TGA analyses, the samples were placed in an alumina ceramic pan and held for one min at 25 °C, and then the temperature was raised to 700 °C at the heating rate of 10 °C/min under the nitrogen flow of 40 mL/min. For SEM and EDX analyses, a JEOL JSM-5910 (Japan) EDX spectrometer with coupled scanning electron microscope EDX was used. The samples were stuck with carbon conducting tape on sample stub and sputtered with gold in fine coater (SPI-module) for 30 s. The stubs bearing samples were inserted in the sample chamber of the instrument. The machine was evacuated and morphology of the samples was investigated. The SEM images were obtained at accelerating voltage of 10 kV, while the distance of the sample from the tip of electron gun was 10 mm and EDX spectrum was recorded using 10 keV. UV/visible spectra were recorded using Lambda 650 PerkinElmer (USA) double beam UV/visible spectrophotometer.

5. Electrical Properties

The electrical properties of the materials were determined using an LCR-meter (GW INSTEK LCR-817, Taiwan) at applied voltage of 1 V and frequency of 1 kHz. For this purpose, interdigitated electrodes of copper were locally prepared on a printed circuit board having a gap of ~93 μm between the fingers. A known amount (0.05 g) of each sample was dispersed in acetone (1 mL) by sonication for 30 min at room temperature. The samples were then deposited on the electrode by drop-casting method by dropping 0.5 mL of the suspension onto the surface of the electrode. The coated electrode was placed in an oven at 40 °C for 30 min to remove the acetone. The sample-coated electrode was attached to the LCR-meter through crocodiles and subjected to the study of electrical properties. The effect of V_2O_5 content in the composites and temperature (20-70 °C) on the electrical properties of samples was also investigated.

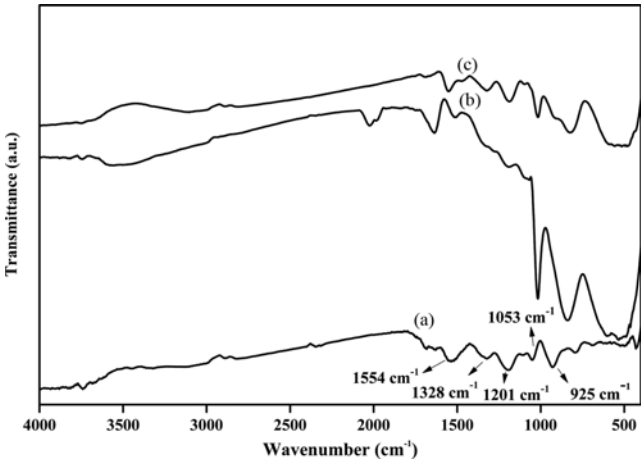

Fig. 2. FT-IR spectra of (a) PPy (b) V_2O_5 and (c) PPy/2%V_2O_5.

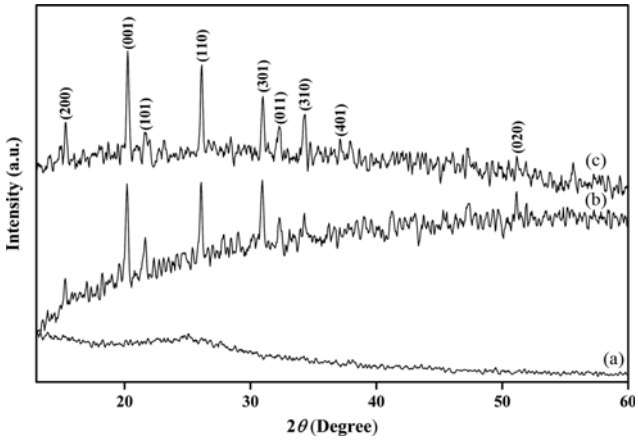

Fig. 3. XRD patterns of (a) PPy (b) V_2O_5 (c) PPy/2%V_2O_5.

RESULTS AND DISCUSSION

1. FT-IR Spectroscopic Analysis

To illustrate the successful synthesis of PPy and co-existence of PPy and V_2O_5, an FT-IR study of the samples was carried out. FT-IR spectra of PPy, V_2O_5 and PPy/2%V_2O_5 are shown in Fig. 2. The synthesis of PPy was established from FT-IR study (Fig. 2(a)). The band at around 1,554 cm^{-1} is allocated to stretching vibration of C=C in the pyrrole ring [31]. The absorption band at 1,328 cm^{-1} is related to C-H in plane deformation modes [32]. The characteristic absorption bands at 1,201 and 1,053 cm^{-1} are, respectively, due to the stretching vibrations of C-N and C-H of PPy [33]. The peak at 925 cm^{-1} is due to the =CH out of plane vibration [34]. Fig. 2(b) shows the FT-IR spectrum of V_2O_5 with absorption bands at 1,022, 842 and 540 cm^{-1}. The band at 1,022 cm^{-1} is due to V=O stretching, and likewise, bands at 842 and 540 cm^{-1} are assigned to V-O-V deformation modes. Similarly, the FT-IR spectrum of PPy/2%V_2O_5 composite shows the characteristic peaks of both the components: PPy and V_2O_5 (Fig. 2(c)). However, the characteristic vibration peaks of V-O-V at 842 and 540 cm^{-1} are slightly shifted to 825 and 557 cm^{-1}, respectively. This shifting may due to some sensitive physical contact between V_2O_5 and PPy [35]. The observed FT-IR results are in good line with the reported results [36].

2. XRD Pattern

XRD patterns of PPy, V_2O_5 and PPy/2%V_2O_5 are shown in Fig. 3(a)-(c). A characteristic peak (Fig. 3(a)) at 2θ from 20 to 30° indicates the amorphous nature of PPy [37] is due to the scattering from the PPy chains at the interplanar spacing [38].

The V_2O_5 is of crystalline nature (Fig. 3(b)), having ICCD PDF-4 Card # 04-008-4555. The characteristic peaks of V_2O_5 are found at 2θ=15.3°, 20.2°, 26.1°, 30.9°, 32.3°, 34.2°, 37.2° and 51.1°, which are allocated to (200), (001), (110), (301), (011), (310), (401) and (020) lattice planes, respectively. In the XRD spectrum of PPy/2%V_2O_5 (Fig. 3(c)), V_2O_5 still reserves good crystallinity and the position of diffraction peaks has no apparent shift.

To find any possible change in the crystallite size of the composites, the average crystallite size of V_2O_5 and the composites was calculated using Debye-Scherrer equation as given below [39,40].

$$L=k\lambda/\beta\cos\theta$$

where L is the average crystallite size, k is the shape factor of value 0.89; θ is the angle of diffraction at the maximum intensity, β is the full width at half maximum of diffraction of angle. The average crystallite size of V_2O_5 was found to be 16.8 nm. Similarly, the average crystallite sizes of the prepared composites are almost the same. It shows that PPy does not alter the crystallinity of V_2O_5, and thus no chemical interface of PPy with V_2O_5 is observed. Thus, the XRD and FT-IR results are in line with each other. The appearance of all the peaks of V_2O_5 in XRD image of the composite confirms the formation of a thin layer of PPy around V_2O_5 particles. The formation of a thin layer is also one of the purposes of this study, because in such a situation both of the components, PPy and V_2O_5, can play their role significantly during their applications in electrical devices [41].

3. TGA

The thermal behavior of the samples is shown in Fig. 4(a)-(f). As is clear from the curve, V_2O_5 is stable and shows no weight loss in the studied temperature range, while the rest of the samples display thermal degradation. In case of PPy (Fig. 4(a)), the initial weight loss around 110 °C is due to the loss of moisture in the sample [42]. The decomposition from 250-440 °C is due to the loss of H, C and N moieties of PPy [18]. The total weight loss due to PPy decomposition is ~72%, while the remaining weight (16%) after PPy degradation is due to carbon residue [30]. The greater thermal stability of PPy, even at higher temperature, is due the greater extent of π-electrons over the heterocyclic ring. The thermal stability of the composites slightly rises with V_2O_5 loading, which is due to the barrier effect of V_2O_5 and lesser movement of polymeric chains when bound on to the particles of V_2O_5. Similarly, with the increase of V_2O_5 content, the water of hydration in the composites has reduced [43]. The TGA curves show that the remaining weight percent of the composites increases from PPy/2%V_2O_5 to PPy/10%V_2O_5, which is due to the increase in the content of V_2O_5. The approximate weight percent of V_2O_5 in the composites was calculated from the TGA results of the composites. From TGA data, after excluding the weight percent of PPy remnants, the weight percent of V_2O_5 in the composites was found to

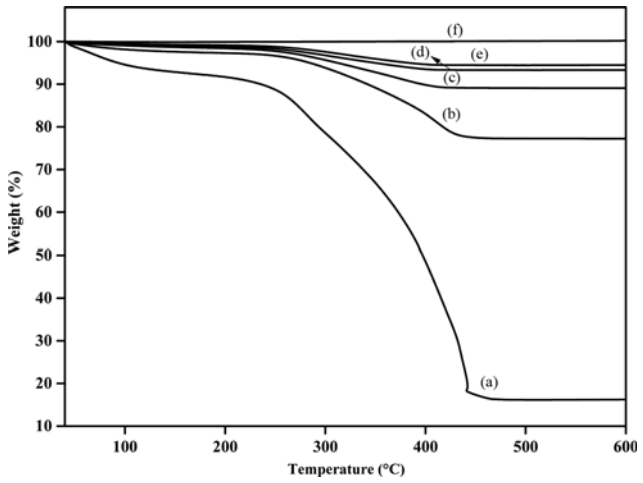

Fig. 4. TGA curves of (a) PPy (b) PPy/2% V_2O_5 (c) PPy/5% V_2O_5 (d) PPy/8%V_2O_5 (e) PPy/10% V_2O_5 and (f) V_2O_5.

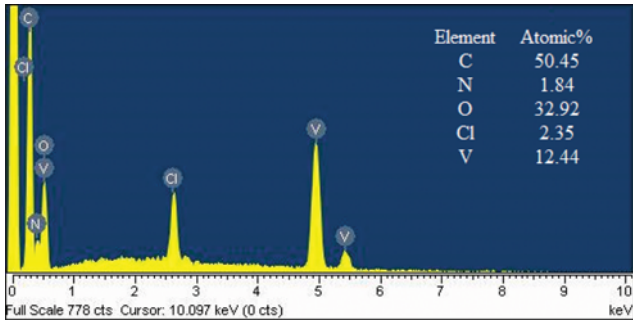

Fig. 5. EDX spectrum of PPy/2%V_2O_5.

be around 61, 73, 77 and 78% for PPy/2%V_2O_5, PPy/5%V_2O_5, PPy/8%V_2O_5 and PPy/10%V_2O_5, respectively. The EDX spectrum of PPy/2%V_2O_5 is shown in Fig. 5. From the EDX spectral analysis, the atomic percentages of V, O, C, N and Cl in the composite (PPy/2%V_2O_5) are 12.44, 32.92, 50.45, 1.84 and 2.35%, respectively. Thus, the molar ratio of C, N, Cl and V_2O_5 was 50.45 : 1.84 : 2.35 : 6.22, respectively. These results show that the actual amount of V_2O_5 in the composite is greater than the added amount. Similarly, the actual amount of V_2O_5 in other composites is also found greater than the added amount. As mentioned, we were interested in the composites with a thin layer of PPy on around V_2O_5 particles. Therefore, we used smaller concentration of the reactants (Py and $FeCl_3 \cdot 6H_2O$) at the start, which resulted in a relatively smaller yield of PPy. Thus, this difference between the added amount of V_2O_5 and the actual amount in the composites is according to our expectations.

To further verify the effect of V_2O_5 contents on the thermal stability of the composites, the activation energy of the decomposition of PPy and PP/V_2O_5 composites was determined by using a well-known integral Broido method [44,45].

$$\ln\ln\left(\frac{1}{Y}\right) = -\left(\frac{E}{R}\right)\frac{1}{T} + \text{constant}$$

where $Y = w_t - w_f / w_0 - w_f$ and is the fraction of the sample not yet

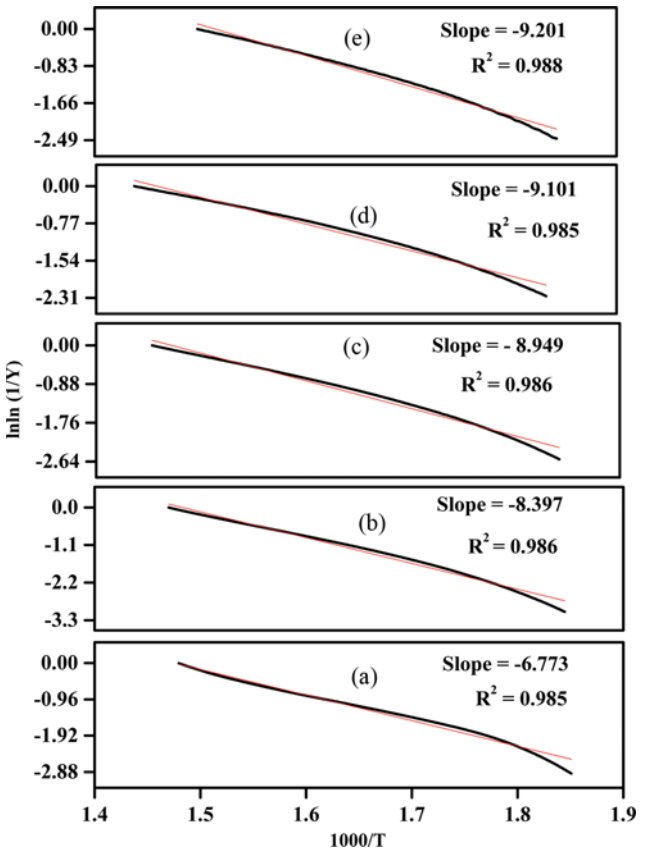

Fig. 6. Activation energy plot of (a) PPy (b) PPy/2%V_2O_5 (c) PPy/5%V_2O_5 (d) PPy/8%V_2O_5 (e) PPy/10%V_2O_5.

Table 1. Activation energy of PPy and PPy/V_2O_5 composites

Sample	Activation energy (kJ/mol)
PPy	56.3
PPy/2%V_2O_5	69.8
PPy/5%V_2O_5	74.4
PPy/8%V_2O_5	75.6
PPy/10%V_2O_5	76.5

decomposed, w_t is the weight at any time t, w_f is the final weight and w_o is the initial weight. The plots for the calculation of activation energy by this method are shown in Fig. 6. The slope of the plot of lnln(1/Y) *vs* 1/T is related to the activation energy. The values of the activation energy of the samples were determined and presented in Table 1. The activation energy increases from PPy to PPy/10%V_2O_5 and hence the thermal stability. These results also suggest some possible interactions between PPy backbone and V_2O_5 particles, which is consistent with FT-IR results.

4. SEM Analysis

SEM images of the samples show complete encapsulation of V_2O_5 in PPy matrix (Fig. 7). The morphology of PPy is hemispherical with globular shaped particles. The average grain size of PPy is ~0.5 μm (Fig. 7(a)). By adding V_2O_5 (2 wt%), the compactness of the PPy/2%V_2O_5 has greatly increased as compared to PPy (Fig. 7(b)). The particles of PPy/2%V_2O_5 are well-interlinked. Due to

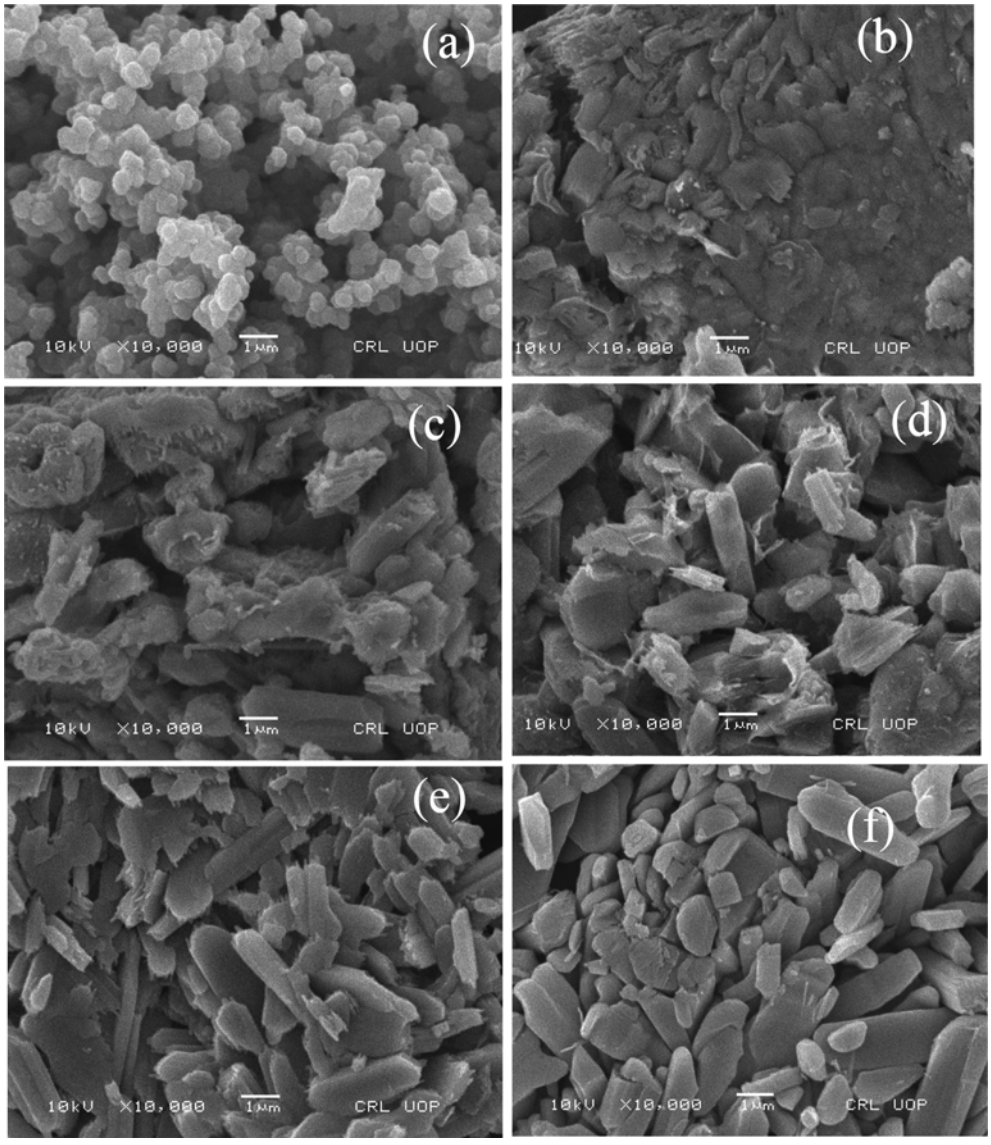

Fig. 7. SEM images of (a) PPy (b) PPy/2%V_2O_5 (c) PPy/5%V_2O_5 (d) PPy/8%V_2O_5, (e) PPy/10%V_2O_5 and (f) V_2O_5.

the encapsulation of V_2O_5 particles, the porosity of PPy has been enhanced in the composite. However, further increase in V_2O_5 content results in the segregation of the composites particles (Fig. 7(c)-(e)). This may be due to the relatively increased proportion of V_2O_5 as these particles are of dispersed nature (Fig. 7(f)). The PPy coating can be clearly seen around the V_2O_5 particles, as Py is polymerized around the particles of V_2O_5. Since the composites are obtained by mixing solid V_2O_5 with Py, the morphology of all the composites is almost the same, i.e., rod shaped. The preservation of the core particles morphology in the composites is because of the formation of a PPy thin layer around V_2O_5 particles, which is in line with XRD results. Similar maintenance of surface morphology of the core particles in the composites was also reported for the chitosan conjugated magnetic nanoparticles [46].

5. Effect of V_2O_5 Content on the Electrical Properties of PPy Composites

The electrical properties in the form of resistance of PPy and PPy/V_2O_5 composites were studied at room temperature, as depicted in Fig. 8. Initially, the resistance decreases significantly from PPy to PPy/2%V_2O_5 and then slightly increases from PPy/5%V_2O_5 to PPy/10%V_2O_5. The higher resistance of PPy is due to the porous nature of its particles and weak linkage among the polymeric particles through the grain boundaries [30], which restricts the movement of charge carriers. In the present study, higher resistance values of PPy were obtained as compared to the reported literature [47]. The conductivity of PPy depends on several other factors, such as the nature of the solvent, concentration of the oxidant, polymerization type, time and temperature [48,49]. Among these parameters, the nature of the solvent, concentration of the oxidant and polymerization temperature play key role in reducing the resistance of PPy. Rodriquez et al. [50] reported the yield of PPy films with higher conductivity (lower resistance) in aqueous medium at lower temperature (0-5 °C). Similarly, the optimum oxidant/monomer ratio for the synthesis of PPy of lower resistance by chemical

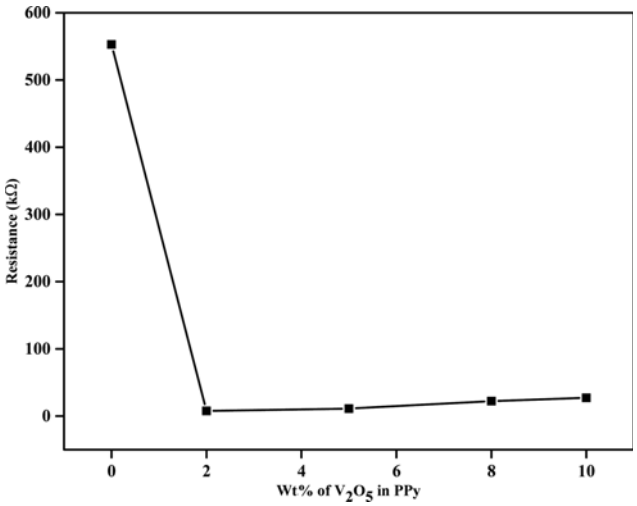

Fig. 8. Effect of V_2O_5 content on the resistance of PPy and its V_2O_5 composites.

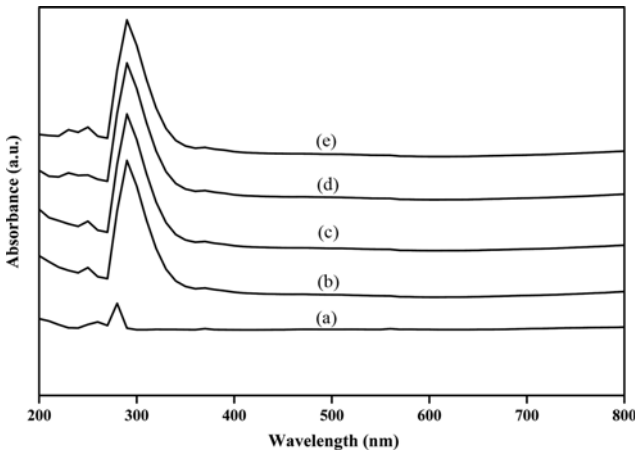

Fig. 9. UV/visible spectra of (a) PPy (b) PPy/2%V_2O_5 (c) PPy/5%V_2O_5 (d) PPy/8%V_2O_5 and (e) PPy/10%V_2O_5.

polymerization using $FeCl_3$ as an oxidant is reported to be 2.2-2.3 [51]. In the present study, we used relatively higher polymerization temperature (8 °C) and lower concentration of the oxidant (0.1 M). These experimental conditions may have also increased the resistance of the resultant PPy. By adding V_2O_5 particles, conjugation and connection through the grain boundaries of the polymer chain increases to facilitate the charge carrier's motion [52], which results in the decrease of electrical resistance. Therefore, PPy/2%V_2O_5 shows the smallest electrical resistance among all the samples. It means that adding V_2O_5 particles of this level (2%) expedites the movement of charge carriers through the polymeric chains and provides good physiochemical connections between PPy and V_2O_5 particles. However, increasing V_2O_5 content beyond 2%, the resistance slightly increased (PPy/5%V_2O_5 to PPy/10%V_2O_5). This may be due to the accumulation of charge carriers [53] owing to the increase in the segregation of the samples particles. This can be explained by the fact that on one hand, V_2O_5 particles hamper the transport of charge carriers among different conjugated chains of PPy, and on the other hand, the existence of an interface between PPy and V_2O_5 particles results in the decrease of conjugation lengths in PPy chains. The decrease in the resistance of the composites, as compared to PPy, suggests the increase in the mobility of charge carriers in the composites. The variation of samples resistance with their compactness is in good line with the SEM results. To find the effect of V_2O_5 particles on the doping of PPy, UV/visible spectra of PPy and PPy/V_2O_5 composites dispersed in ethanol were recorded from 200 to 800 nm (Fig. 9). The spectrum of PPy exhibits a distinct absorption peak at 279 nm, which is attributed to π to π^* of transition of the benzenoid ring. All the synthesized composites also show the absorption peak with a shift to 289 nm, which may be due to the successful interaction of metal oxide particles with the polymer chains [54]. The similarity in the absorption peaks of the composites suggests that after adding 2 wt% of V_2O_5, there is no effect of V_2O_5 content on the λ_{max} of the composites. This indicates that 2 wt% of V_2O_5 is sufficient for the synthesis of a PPy/V_2O_5 composite of optimized properties in the present case. The band gap energy of PPy and PPy/V_2O_5 composites is calculated by using the following equation [55]:

$$E_g = hc/\lambda$$

where E_g is the band gap energy, h is Planck's constant, C is the speed of light and λ is the cut-off wavelength, which is 290 nm for PPy and 351 nm for the composites. The band gap energy values for PPy and PPy/V_2O_5 composites were found to be 3.89 and 3.22 eV, respectively. The smaller band gap energy value of the composites indicates the relatively higher doping of PPy in the composites as compared to the pure PPy. The difference in the band gap energy values of PPy and the composites is not as much as the resistance differences (Fig. 8). Thus, it is suggested that both the compactness of the sample as well as the doping of PPy in the composites plays a key role in the decrease of composites' resistance. The effect of sample compactness is also clear from the fact that though the band gap energy of the rest of the composites is similar to PPy/2%V_2O_5, however, their resistance increases slightly, which may be due to the decrease in their compactness.

6. Effect of Temperature on the Electrical Resistance of the Samples

To study the effect of temperature on the resistance of the samples, the electrode bearing the sample was placed in a specially designed chamber inside the furnace. The temperature was varied from 20 to 70 °C. The dependence of resistance on temperature is shown in Fig. 10. As the figures show, the resistance of all the samples decreases and hence conductivity increases with the rise in temperature. Thus, the thermal activated behavior of the samples is confirmed. In case of PPy, the decrease in resistance with temperature is due to the increase in charge transfer efficiency [56,57]. It is also suggested that with the rise in temperature, the lattice vibration in PPy increases, which results in chain stretching. The stretching of the chains results in an effective charge spreading all over the chain and improvement in arrangement of polymer chains with capacity for longer conjugation length. This results in the intra- and interchain hopping of charge carriers, which in turn lowers the resistance [53]. Also, with heating there will be molecular rearrangement in PPy, which makes the molecules more favor-

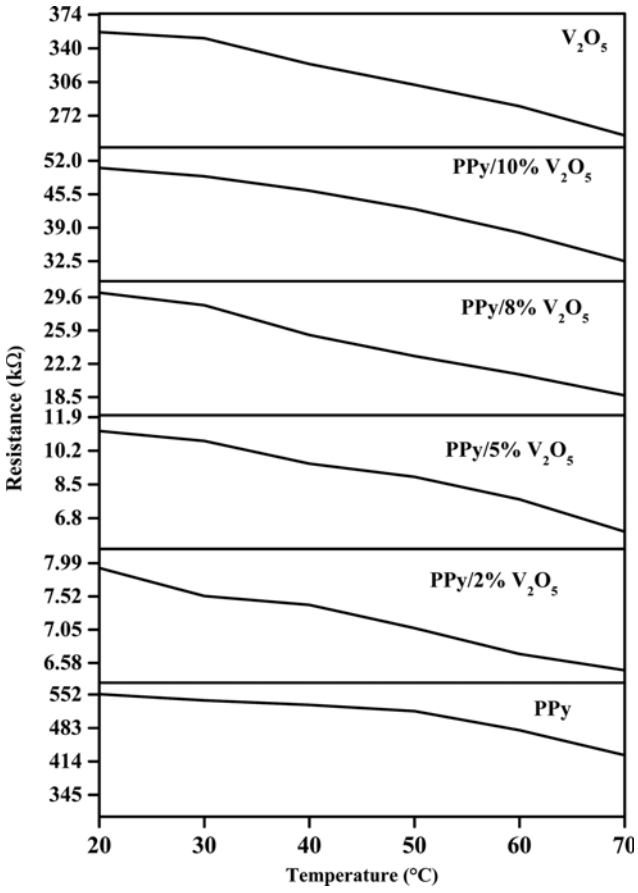

Fig. 10. Effect of temperature on the resistance of PPy and its V_2O_5 composites.

able for the charge carrier's moment [58]. Similarly, for the composites contain semiconducting V_2O_5, and there is physical interaction between PPy and V_2O_5 particles, therefore, the resistance of the composites decreases with temperature. The effect of temperature on resistance of the samples reveals their semiconducting nature [59].

CONCLUSIONS

A simple route was followed for the synthesis of PPy and PPy/V_2O_5 composites in aqueous medium at room temperature using chemical oxidation polymerization. The structure, thermal stability, surface morphology and electrical properties of the samples were investigated. The composites showed substantial improvement in their electrical characteristics. The FT-IR report confirmed a sort of sensitive physical interaction of PPy with V_2O_5 in the resultant composites. From the XRD study, PPy is amorphous and its V_2O_5 composites are crystalline. The V_2O_5 loading of 2% was found to be the optimized value for the preparation of PPy/V_2O_5 with good compactness and smallest resistance. The resistance decreases from PPy to PPy/2%V_2O_5 and then increases due to the segregation of samples particles and doping of PPy. Due to the easy synthetic protocol and good electrical properties of the materials presented herein, it would of great interest if further research is carried out to investigate the applications of these materials as gas sensor, which is our next goal.

REFERENCES

1. V. K. Gade, D. J. Shirale, P. D. Gaikwad, K. P. Kakde, P. A. Savale, H. J. Kharat, B. H. Pawar and M. D. Shirsat, *Int. J. Electrochem. Sci.*, **2**, 270 (2007).
2. H. Zengin and B. Erkan, *Polym. Adv. Technol.*, **21**, 216 (2010).
3. J. C. Vidal, E. Garcia and J. R. Castillo, *Anal. Chem. Acta*, **385**, 213 (1999).
4. T. E. Campbell, A. J. Hodgson and G. G. Wallace, *Electroanalysis*, **11**, 215 (1999).
5. D. Kincal, A. Kumar, A. D. Child and J. R. Reynolds, *Synth. Met.*, **92**, 53 (1998).
6. N. T. Kemp, G. U. Flanagan, A. B. Kaiser, H. J. Trodahl, B. Chapman, A. C. Partridge and R. G. Buckley, *Synth. Met.*, **101**, 434 (1999).
7. C. Jerome, D. Labaye, I. Bodart and R. Jerome, *Synth. Met.*, **101**, 3 (1999).
8. E. Smela, *J. Micromech. Microeng.*, **9**, 1 (1999).
9. G. S. Akundy, R. Rajagopalan and J. O. Iroh, *J. Appl. Polym. Sci.*, **83**, 1970 (2002).
10. T. Ito, P. Buehlmann and Y. Umezawa, *Anal. Chem.*, **71**, 1699 (1999).
11. X. Feng, Z. Sun, W. Hou and J.-J. Zhu, *Nanotechnology*, **18**, 1 (2007).
12. J. Jiang, L. Ai and L. Li, *J. Phys. Chem. B*, **113**, 1376 (2009).
13. J. Jiang and L. H. Ai, *J. Mater. Sci.*, **21**, 687 (2010).
14. H. Li, Y. Jia, S. Luan, Q. Xiang, C. C. Han, G. Mamtin, Y. Han and L. An, *Polym. Compos.*, **29**, 649 (2008).
15. A. Bhattacharaya, D. C. Mukherjee, J. M. Gohil, Y. Kumar and S. Kundu, *Desalination*, **225**, 366 (2008).
16. P. P. Sengupta, P. Kar and B. A. Dhikari, *Thin Solid Films*, **517**, 3770 (2009).
17. S. C. Hernandez, D. Chaudhuri, W. Chen, N. V. Myung and A. Mulchandani, *Electroanalysis*, **19**, 2125 (2007).
18. K. Majid, R. Tabassum, A. F. Shah, S. Ahmad and M. L. Singla, *J. Mater. Sci.: Mater. Electron.*, **20**, 958 (2009).
19. H. Yuvaraj, E. J. Park, Y.-S. Gal and K. T. Lim, *Colloid. Surf., A*, **300**, 313 (2008).
20. F. Kanwal, S. A. Siddiqi, A. Batool, M. Imran, W. Mushtaq and T. Jamil, *Synth. Met.*, **161**, 335 (2011).
21. I. Boyano, M. Bengoechea, I. de Meatza, O. Miguel, I. Cantero, E. Ochoteco, J.odrıguez, M. Lira-Cantu and P. Gomez-Romero, *J. Power Sources*, **166**, 471 (2007).
22. S. Kuwabata, S. Masui, H. Tomiyori and H. Yoneyam, *Electrochim. Acta*, **46**, 91 (2000).
23. X. Sun, Q. Li and Y. Mao, *Electrochim. Acta*, **174**, 563 (2015).
24. N. Abd. Rahman, T. I. T. Kudin, Ab. M. M. Ali and M. Z. A. Yahya, *J. Mater. Sci Eng. B*, **1**, 457 (2011).
25. C. Basavaraja, E. A. Jo, B. S. Kim, D. G. Kim and D. S. Huh, *Macromol. Res.*, **18**, 1037 (2010).
26. A. Varesano, C. Tonin, F. Ferrero and M. Stringhetta, *J. Therm. Anal. Calorim.*, **94**, 559 (2008).
27. R. Ansari, *E-J. Chem.*, **3**, 186 (2006).

28. Y. He, T. Sheng, J. Chen, R. Fu, S. Hu and X. Wu, *Catal. Commun.*, **10**, 1354 (2009).
29. C. Xiong, A. E. Aliev, B. Gnade and K. J. Balkus, *ACS Nano*, **2**, 293 (2008).
30. A. Batool, F. Kanwal, M. Imran, T. J. Saadat and A. Siddiqi, *Synth. Met.*, **161**, 2753 (2012).
31. M. Selvarage, S. Palraj, K. Murathan, G. Rajagopal and G. Venkatachari, *Synth. Met.*, **158**, 888 (2008).
32. Y. Li, R. Yi, A. Yan, L. Deng, K. Zhou and X. Liu, *Solid State Sci.*, **11**, 1319 (2009).
33. Y. Han, *Polym. Compos.*, **30**, 66 (2009).
34. M. T. Ramesan, *J. Appl. Polym. Sci.*, **128**, 1540 (2013).
35. H. Zhao, A. Yuan, B. Liu, S. Xing, X. Wu and J. Xu, *J. Appl. Electrochem.*, **42**, 139 (2012).
36. Y. Kim, J. S. Kim, M. T. Thieu, H. C. Dinh, I. H. Yeo, W. Cho and S. Mho, *Bull. Korean Chem. Soc.*, **31**, 3110 (2010).
37. N. S. Allena, K. S. Murray, R. J. Fleming and B. R. Saunders, *Synth. Met.*, **87**, 237 (1997).
38. J. Y. Ouyang and Y. F. Li, *Polymer*, **15**, 3997 (1997).
39. A. Aytimur, I. Uslu, S. Kocyigit and F. Ozcan, *Ceram. Int.*, **38**, 3851 (2012).
40. K. M. Parida, A. C. Pradhan, J. Das and N. Sahu, *Mater. Chem. Phys.*, **113**, 244 (2009).
41. X. Ren, C. Shi, P. Zhang, Y. Jiang, J. Liu and Q. Zhang, *Mater. Sci. Eng.*, **177**, 929 (2012).
42. Z. Guo, K. Shin, A. B. Karki, D. P. Young and R. B. Kaner, *J. Nanopart. Res.*, **11**, 1441 (2009).
43. J. Zhu, S. Wei, L. Zhang, Y. Mao, J. Ryu, P. Mavinakuli, A. B. Karki, D. P. Young and Z. Guo, *J. Phys. Chem. C*, **114**, 16335 (2010).
44. S. Gopalakrishnan and R. Sujatha, *Der. Chem. Sinica*, **2**, 103 (2011).
45. P. S. Abthagir, R. Saraswathi and S. Sivakolunthu, *Therm. Chem. Acta*, **2**, 109 (2004).
46. H. Khan, A. K. Khalil, A. Khan, K. Saeed and N. Ali, *Korean J. Chem. Eng.*, **33**, 2802 (2016).
47. M. A. Chougule, S. G. Pawar, P. R. Godse, R. N. Mulik, S. Sen and V. B. Patil, *Soft Nanosci. Lett.*, **1**, 6 (2011).
48. S. Machida and S. Miyata, *Synth. Met.*, **31**, 311 (1989).
49. S. Rapi, V. Bocchi and G. P. Gardini, *Synth. Met.*, **24**, 217 (1988).
50. J. Rodriquez, J. J. Grande and T. F. Otero, Handbook of Organic Conductive Molecules and Polymers, In: *Conductive Polymers: Synthesis and Electrical Properties*, H. S. Nalwa Ed., Vol. 2, Chapter 10, p. 413, Wiley, New York (1997).
51. Y. Kudoh, *Synth. Met.*, **79**, 17 (1996).
52. M. S. Bhende, S. P. Yawale and S. S. Yawale, *IJIERE*, **3**, 488 (2016).
53. M. A. Chougule, G. D. Khuspe, S. Sen and V. B. Patil, *Appl. Nanosci.*, **3**, 423 (2013).
54. M. Alam, A. A. Ansari, M. R. Shaik and N. M. Alandis, *Arab. J. Chem.*, **6**, 341 (2013).
55. C. Piewnuan, J. Wootthikanokkhan, P. Ngaotrakanwiwat, V. Meeyoo and S. Chiarakorn, *Superlatt. Microstruct.*, **75**, 105 (2014).
56. M. Leclerc, G. D. Aparno and G. Zotti, *Synth. Met.*, **2**, 1527 (1993).
57. F. Zuo, M. Angelopoulos, A. G. MacDiarmid and A. J. Epstein, *Phys. Rev. B*, **5**, 3475 (1987).
58. A. Kobayashi, H. Ishikawa, K. Amano, M. Satoh and E. Hasegawa, *J. Appl. Phys.*, **1**, 296 (1993).
59. T. Fatima, T. Sankarappa and R. Ramanna, *IJARPS*, **3**, 7 (2016).